Construction and analysis of cortical–muscular functional network based on EEG-EMG coherence using wavelet coherence

Xugang Xi [a,b,*], Ziyang Sun [a,b], Xian Hua [c], Changmin Yuan [a,b], Yun-Bo Zhao [d], Seyed M. Miran [e], Zhizeng Luo [a], Zhong Lü [f,*]

[a] School of Automation, Hangzhou Dianzi University, Hangzhou 310018, China
[b] Key Laboratory of Brain Machine Collaborative Intelligence of Zhejiang Province, Hangzhou 310018, China
[c] Jinhua People's Hospital, Jinhua 321000, China
[d] Department of Automation, Zhejiang University of Technology, Hangzhou 310023, China
[e] Biomedical Informatics Center, George Washington University, Washington, DC 20052, USA
[f] Affiliated Dongyang Hospital of Wenzhou Medical University, Dongyang 322100, China

ARTICLE INFO

ABSTRACT

Research on the brain functional network is important in understanding the normal function of the brain and diagnosing neuropsychiatric diseases. Inspired by the brain functional network, we constructed a cortical–muscular functional network using electroencephalography and electromyography to explore the motion control mechanism of the central nervous system and understand the organization and coordination mechanisms of limb motion control. In the process of constructing the network, 12 signal acquisition channels were selected as nodes, and the wavelet coherence is used as the index of connection between network nodes. Based on the original network, we used a fixed weighted edge and threshold methods to remove weak weighted edges and compare the performance of the two methods. The experimental results showed that the constructed network had a higher clustering coefficient, and the smaller characteristic path length indicated a small-world characteristic. At the same time, the weighted characteristic path length and weighted clustering coefficient of the functional network simplified by the threshold method can show promising classification accuracy under Fisher and artificial neural network.

© 2021 Elsevier B.V. All rights reserved.

1. Introduction

The synchronization between Electroencephalography (EEG) and surface electromyography (sEMG) signals in neural motor control can reflect the functional link between the cortex and the muscle, and the EEG of the motor cortex and the sEMG of the contralateral muscle can reflect, respectively, the motion control information and the response of the muscle to the brain's control intention. It has thus become popular in the field of motor neuroscience to study the coupling of cortex and muscle, and consequently the relationship between the motion control and response mechanism during exercise. Useful EEG signals are mainly distributed in the 1–80 Hz range (delta: 1–3 Hz, theta: 4–7 Hz, alpha: 8–13 Hz, beta: 14–30 Hz, gamma: 30–80 Hz), and the range of magnitude is 5–200 μV. EEG is a reflection of the electrical activity between brain tissues and the functional status of

various brain regions, and it is crucial in understanding the information processing process of the brain. Useful sEMG signals are mainly distributed in the 10–500 Hz range, and the range of magnitude is 100–5000 μV. As a resource of the human body, sEMG signals contain rich information on human movement and are ideal control signals for artificial limbs and functional nerve electrical stimulation [1,2]. EEG is widely used in neurological diseases, [3,4] brain-machine interface, [5–7] and motor imagery, and sEMG is utilized in rehabilitation training, [8,9] medical sensing, [10] mechanical control, [11,12] and many other fields.

In the process of human autonomous movement, synergy occurs between different regions of the brain. In accordance with that, researchers have proposed the brain function networks based on this characteristic. In the past 20 years, after introducing the small-world features of most real networks [13] and the scale-free features of large-scale networks, [14] brain functional networks have developed rapidly. At present, brain function networks have been widely used in the brain sciences to study different brain functions or dysfunctions [15–18]. In addition to the brain regions, people found that the motor cortex, brain somatosensory

---

* Corresponding authors at: School of Automation, Hangzhou Dianzi University, Hangzhou 310018, China (Xugang Xi).

E-mail address: xixi@hdu.edu.cn (X. Xi).

cortex and motor muscle tissue nerve cells automatically synchronize [19,20]. The coherence between cortical and muscle activities varies with the function of cortical involvement in different tasks. The coherence between EEG and sEMG in the beta frequency band (13–30 Hz) is pronounced during visuomotor tasks [21–23] and low during automatic postural functions [24]. The coherence between EEG and sEMG in the gamma frequency band (30–45 Hz) is pronounced during dynamic [23] and intense contractions [25]. The interaction between the cortex, motor nerves and muscle tissue is called cortical-muscle functional coupling (CMC). In recent years, more and more researchers have conducted research on CMC. Mima and Hallett described the CMC mechanism and extracted coherence between EEG and sEMG produced by the right abductor pollicis brevis muscle [26–28]. Chen et al. [29] proposed a time–frequency transfer entropy algorithm based on harmonic wavelet transform and symbol phase transfer entropy, revealing that the cortical muscle motor system controls muscle strength by regulating the synchronous oscillation of neurons. Bao et al. [28] studied the possibility of High-Definition Transcranial Direct Current Stimulation (hd-tdcs) combined with EEG and found that the anode hd-tdcs caused significant changes in CMC in stroke patients while the cathode and sham stimulation did not. The research studies on CMC mainly adopt methods such as coherence analysis, phase synchronization index, generalized synchronization index, Granger causality measure, information theory measure and so on. Among them, coherence analysis is one of the most widely used methods. Coherence estimation is a measure of the functional connectivity between different sources of neuro-oscillatory activity through the correlation degree between sites (e.g., cortical and muscle) in the frequency domain [20,30–35]. The wavelet coherence (WC) method has shown good results in studying the coupling of EEG and EMG signals [26,27]. Using WC to analyze CMC can provide a theoretical basis for motion control, feedback information decoding and clinical rehabilitation assessment. This will help to explore the central nervous system movement control mechanism and understand the organization's coordination mechanism in the process of limb movement control.

In this study, with the help of the brain function network and the method of studying CMC, we started from the mechanism of human movement and used WC as the connection between cortical and muscle functions and constructed a brain-muscle function network. The proposed functional network can display the characteristics of the signal in the time domain and the frequency domain, and has significant advantages and potential in decoding human motion intentions. We calculated the weighted edges of the function networks by studying CMC and preliminarily selected the WC value as the cortical–muscular functional connectivity. The threshold method (THR) and fixed weighted edge method (FWE) were used to delete weak weighted edges. Then, we checked if the cortical–muscular functional network had small-world characteristics. Applying this network to the motion recognition, the experimental results showed that the network is effective indicating substantial significance for exploring the motion control mechanism of the central nervous system and understanding the organization and coordination mechanism of limb motion control.

The remainder of this paper is organized as follows. Section 2 presents the proposed network in detail. Section 3 discusses the experimental results. Section 4 provides the conclusions.

2. Materials and methods

2.1. Subjects

We recruited seven healthy male and seven healthy female participants who were right-handed. The age of the participants ranged from 22 to 25, and their body mass index was from 19.0 to 22.6. The subjects had no neurological history, were informed of the details of the experiment, and signed an informed consent form. Before the experiment, the participants were required to satisfy the following: (1) they lead a regular life routine, (2) they do not stay up late, (3) they did not take alcoholic drinks or drugs a week before the experiment, (4) they did not smoke or drink coffee or strong tea eight hours before the experiment, and (5) they washed their hair two hours before the experiment. The entire process followed relevant ethical standards.

2.2. Acquisition and processing of EEG and sEMG data

EEG data were recorded by a digital EEG apparatus (g.MOBllab + MP-2015) at the following eight positions of the 10–20 systems: C1, C2, C3, C4, C5, FC1, FC3, and CP1 (Fpz was selected as the grounding electrode). Considering that all the subjects were right-handed, some of the electrodes only took in the left brain region to build a much leaner function network. EMG signals were recorded by Trigno™ Wireless EMG (Delsys Inc, Natick, MA, USA). Bluetooth was used as the communication protocol, and motion artifact suppression could be freely movable. The sampling frequency of the sEMG signals was 1600 Hz using EMG Works 4.0 acquisition software (DelSys, Inc., Natick, MA, USA). The sEMG signals were recorded by four surface electrodes on the muscles of the right upper limb (extensor digitorum, flexor carpi radialis, flexor digitorum superficialis, and extensor carpi ulnaris). All data is denoised by wavelet de-noising to remove noise, and EEG also removes electrooculogram (EOG) via ICA algorithm.

Three gestures, namely, wrist flexion (WF), wrist extension (WE) and clench fist (CF), were considered in the EEG and sEMG data acquisition. We asked each subject to do each pose for 30 s followed by one minute rest, and repeat for 20 times. In the end, a total of 840 sets of data were collected, with artifacts being removed through the toolbox. All the collected data are equipped with the de-noising function of the acquisition tool to remove noise interference. The experimental process is shown in Fig. 1.

2.3. Computation of WC

We constructed the cortical–muscular functional network on the basis of the weights of the cortical–muscle functional connectivity. WC was used as the weights of the cortical–muscle functional connectivity and calculated as follows:

(1) The wavelet power (WP) is defined as CWT's norm square of signal x, i,e,

$$WP_x(t,f) = \parallel CWT_x(t,f) \parallel^2 \tag{1}$$

Fig. 1. Data acquisition experiment.

where WP is a function of time t and wavelet center frequency f. CWT stands for continuous wavelet transform.

(2) Cross-wavelet transform (XWT) between signals x and y is defined as

$$XWT_{xy}(t,f) = CWT_x(t,f) \cdot CWT_y^*(t,f) \qquad (2)$$

(3) Similar to the estimation of conventional coherence, a smoothing process was used to estimate WC following the method of Lachaux et al,. [34] Grinsted et al,. [37–39] and Torrence et al. [40]. The smoothing process depends on the wavelet basis and scales. Smoothing operates across scale and time axes, which increases the degree of freedom for each point in CWT [33].

An appropriate smoothing function for WC application across time axis S_{time} is defined as follows using the Morlet wavelet [39].

$$S_{time}(CWT_x(t,f)) = CWT_x(t,f) \wedge c_1^{\frac{-\lambda^2}{2}} \qquad (3)$$

where $\lambda = t/a$, c_1 is a normalization constant, and $\wedge$ refers to the convolution operator. The smoothing function across scale axis S_{scale} is defined as that in, [36] i.e.,

$$S_{scale}(CWT_x(t,f)) = CWT_x(t,f) \wedge c_2 \Pi(0.6a) \qquad (4)$$

where c_2 is a normalization constant and $\prod$ is the rectangular function. a is the scale. In practice, the convolutions in Eqs. (3) and (4) are calculated discretely, and the normalization coefficients are determined numerically. The rectangular function's width used in S_{scale} is determined by the scale–decorrelation length, which electrooculogram to 0.6 [26].

(4) WC is defined as follows by using the smoothing functions.

$$WC_{xy}(t,f) = \frac{\left|S(a^{-1}XWT_{xy}(t,f))\right|^2}{S(a^{-1}WP_x(t,f))S(a^{-1}WP_y(t,f))} \qquad (5)$$

where a^{-1} denotes the scale inverse, which is used to normalize the XWT. Schwartz inequality ensures that $WC_{xy} \in [0,1]$. The smoothing process S is defined as follows:

$$S(w) = S_{scale}[S_{time}(W)] \qquad (6)$$

2.4. Cortical–muscular function network modeling

The algorithm of modeling the brain muscular functional network involves the following steps.

(1) The WC values between the two channels are calculated, and the adjacency matrix is obtained.
(2) The adjacency matrix is divided into three parts, namely, EEG-EEG, EMG-EMG, and EEG-EMG. The WC values of each part are normalized, and a normalized adjacency matrix is obtained.
(3) HR or FWE is employed to delete low weights in the adjacency matrix.

We modeled the cortical–muscular function network by implementing steps (1) to (3) with MATLAB programs. Step (1) aims to calculate the cortical–muscle functional connectivity of every two vertices as the weighted edges. Step (2) standardizes the weighted values because of the connectivity of different kinds of signal differs. Step (3) simplifies the model and highlights the graph characteristics. The brain functional network demonstrates

the functional connectivity between different brain areas. We added sEMG signals to the model to construct the proposed model, namely, the cortical–muscular function network.

2.5. Computation of network characteristics

In complex network theory, a clustering coefficient is a measure of the degree to which nodes in a network tend to cluster together. Clustering coefficient C is defined as follows [41]:

$$C = \frac{1}{N}\sum_{i=1}^{N} C_i \qquad (7)$$

$$C_i = \frac{2E_i}{K_i(K_i - 1)} \qquad (8)$$

where N is the number of vertices, C_i is the clustering coefficient of vertex i, E_i is the number of vertex i and its neighbors that are actually connected with i, and K_i is the degree of vertex i.

Weighted clustering coefficient C^w is defined as follows [19]:

$$C^{wc} = \frac{1}{N}\sum_{i=1}^{N} C_i^{wc}, \qquad (9)$$

$$C_i^{wc} = \frac{1}{K_i(k_i - 1)} \sum_{i \neq j \neq h \in [1,N]} \frac{(wc_{ij} + wc_{ih})}{2} a_{ij}a_{ih}a_{jh} \qquad (10)$$

where k_i is the degree of vertex i in the corresponding binary network, wc_{ij} is the weight of the vertices i, j. a_{ij}, a_{ih} and a_{jh} are the connection between vertices i and j in the corresponding binary network where the connection is 1 and no connections are 0.

Characteristic path length shows the average number of the shortest path between every two vertices and is usually used to measure the global connectivity of networks. Characteristic path length is defined as follows [42]:

$$L = \frac{1}{N(N-1)} \sum_{i \neq j \in [1,N]} l_{ij} \qquad (11)$$

where l_{ij} is the shortest path length between vertices i and.

Weighted characteristic path length L^w is defined as follows [19]:

$$L^{wc} = \frac{1}{n(n-1)} \sum_{i \neq j \in N} l_{ij}^{wc} \qquad (12)$$

$$l_{ij}^{wc} = \min\left(\frac{1}{wc_{ik}} + \frac{1}{wc_{kf}} + \cdots + \frac{1}{wc_{mn}} + \frac{1}{wc_{nj}}\right) \qquad (13)$$

where l_{ij}^{wc} is the weighted shortest path length between vertices i and j.

3. Experiments and results

3.1. WC and adjacency matrix

In the construction of the network, the nodes of the network are determined. They are the channels of collected signals and the index of the connection between nodes is the wavelet coherence value. Wavelet coherence can express the functional connectivity between different sources of neural oscillatory activities through the degree of correlation. Therefore, the network constructed by using wavelet coherence can express the differences between EEG and EMG as well as the inherent laws, so that the network has better performance ability. We calculated the WC values between every two channels. Twelve channels were involved.

Channels 1–8 represent EEG signals, and channels 9–12 represent sEMG signals. The frequency of EEG and EMG signal acquisition is different, the number of EEG and EMG data in the same frequency band is different, so we need to adjust the frequency resolution to make the EEG and EMG data in different frequency bands have the same number of of points to carry out coherence analysis.

We first perform Fourier transform on EEG and sEMG signals, and adjust the different frequency resolutions in Matlab to keep the same number of data points of EEG and sEMG for the same frequency band. Then, we studied the coupling characteristics between different channels in the four frequency ranges of 4–7 Hz, 8–13 Hz, 14–30 Hz, and 30–80 Hz. For convenience, sEMG signals in the frequency range of 4–7 Hz, 8–13 Hz, 14–30 Hz, and 30–80 Hz are also called theta, alpha, beta, and gamma.

Fig. 2 shows the WC values of EEG-EEG, EMG-EMG, and EEG-EMG in different frequency bands. The WC values of EEG-EEG, EMG-EMG, and EEG-EMG show large differences. For the unification of the following research, we normalized the WC values of each case.

We then constructed the adjacency matrix using the normalized WC values of every two channels. The 12 channels of EEG and EMG are taken as the horizontal and vertical axes of the matrix, and then the WC between every two channels is calculated as the value of the elements in the adjacent matrix. Fig. 3 shows the adjacency matrix's colormap of different motions by using different frequency bands. We use the matrix's difference verification method to subtract two matrices to obtain a new difference matrix, and then find the Euclidean norm of the difference matrix. The result is the distance in the mathematical sense, and the difference between the two matrices can be directly compared. Then, the significance test of the Euclidean norm between different frequency bands and different actions was conducted. We used Excel to analyze the significant difference of Euclidean norm. The analysis method was to conduct an Analysis of Variance (ANOVA) of Euclidean norm between different frequency bands and different actions, and the p-value was selected as the analysis result. This means that the probability of the difference between samples due to the sampling error is less than 0.05, 0.01, 0.001. The results of p-values were statistically calculated in Table 1. It can be seen that significant differences were observed in the adjacency matrix of different motions.

3.2. Construction and simplification of networks

After obtaining the initial adjacency matrix, we preliminarily constructed the network model. Fig. 4(a) shows the model diagram without the weighted edge to explain each part of the model. Fig. 4 (b) shows the model diagram with the complete weighted edge, which was constructed using the initial adjacency matrix.

In our experiment, we used two traditional methods, namely, THR and FEW, to delete the low weights in the adjacency matrix.

Table 1
The difference between different movements and different frequency bands.

	theta	alpha	beta	gamma
WE-WF	1.15E−06	0.29E−06	1.01E−06	1.89E−06
WF-CF	1.62E−06	0.49E−06	0.89E−06	1.26E−06
WE-CF	1.81E−07	0.29E−07	0.76E−06	1.21E−06

The threshold method that we adopted is the local adaptive threshold method, which is to set the threshold value in accordance with the connection strength value at a certain position in the adjacency matrix and the position in the surrounding neighborhood. Generally, the methods to set the threshold value include the local neighborhood mean method and the local neighborhood Gaussian weighting method. The method that we selected for this paper is the neighborhood block mean method. FWE selects a fixed weight to compare whether there is a difference between Lw and Cw of the three actions. If there is a difference, it indicates that the selection of threshold is reasonable. In Fig. 5, K is the average number of the weighted edges of each vertex. Weighted clustering coefficient Cw and weighted characteristic path length Lw are the network characteristics. Fig. 5 shows the changes in Cw and Lw in different motions when $K \in [1, 4]$ and the step size is 0.5.

As can be seen from Fig. 5, when K is greater than 2, Lw between the three actions gradually tends to be the same. Therefore, we choose $K = 2$ as the FWE and remove the weighted edge with K greater than 2. We constructed network models using different sets of data to show Cw and Lw in different frequency bands and the results are shown in Fig. 6.

Fig. 7 shows the changes in Cw and Lw in different motions when $T \in [0.5, 0.9]$ and the step size is 0.01. As it can be seen in Fig. 7, regardless of the threshold value, the Cw gap between different actions is very small, and when the threshold is greater than 0.8, the Lw of the three actions starts to show different trends. To ensure that the selected threshold value will not be small due to experimental error, we chose 0.85 as the threshold value and weighted edges less than 0.85 are removed. We constructed network models using different sets of data to show Cw and Lw in different frequency bands and the results are shown in Fig. 8.

Fig. 4(c)–(e) show the simplified model diagram of the three different motions using THR, and Fig. 4(f)–(h) show the simplified model diagram using FWE. After deleting the low weight, we also conducted a difference analysis on the new network, and the results were shown in Fig. 9. The significant differences are shown in Tables 2 and 3. In these tables, SS means Stdev square, DF means degree freedom and MS means Mean square and the value is equal to the corresponding SS divided by DF. F is the statistic, the statistic used in the analysis of variance for hypothesis testing, and its value is equal to MS of processing divided by MS of error. The p-value is the probability value for the corresponding F value. F-crit is the critical value of F at the corresponding significance level. According
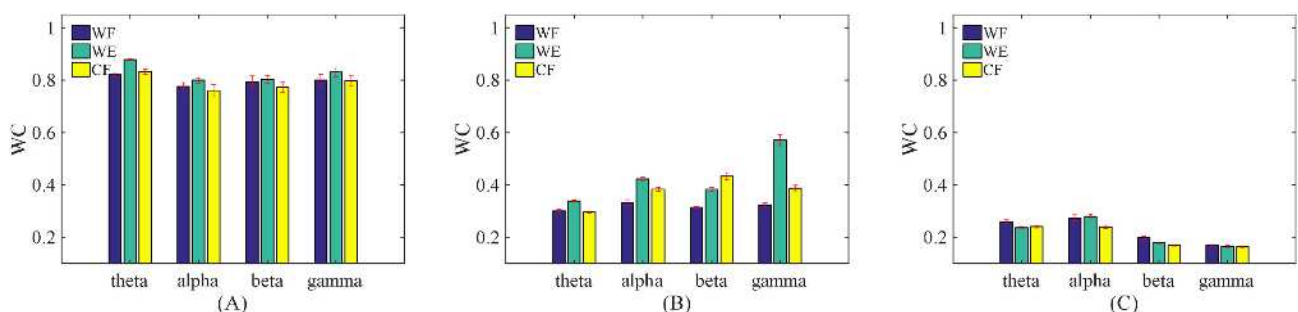

Fig. 2. Wavelet coherence values of EEG-EEG, EMG-EMG, and EEG-EMG in different frequency bands. (A) EEG-EEG, (B) EMG-EMG, and (C) EEG-EMG.
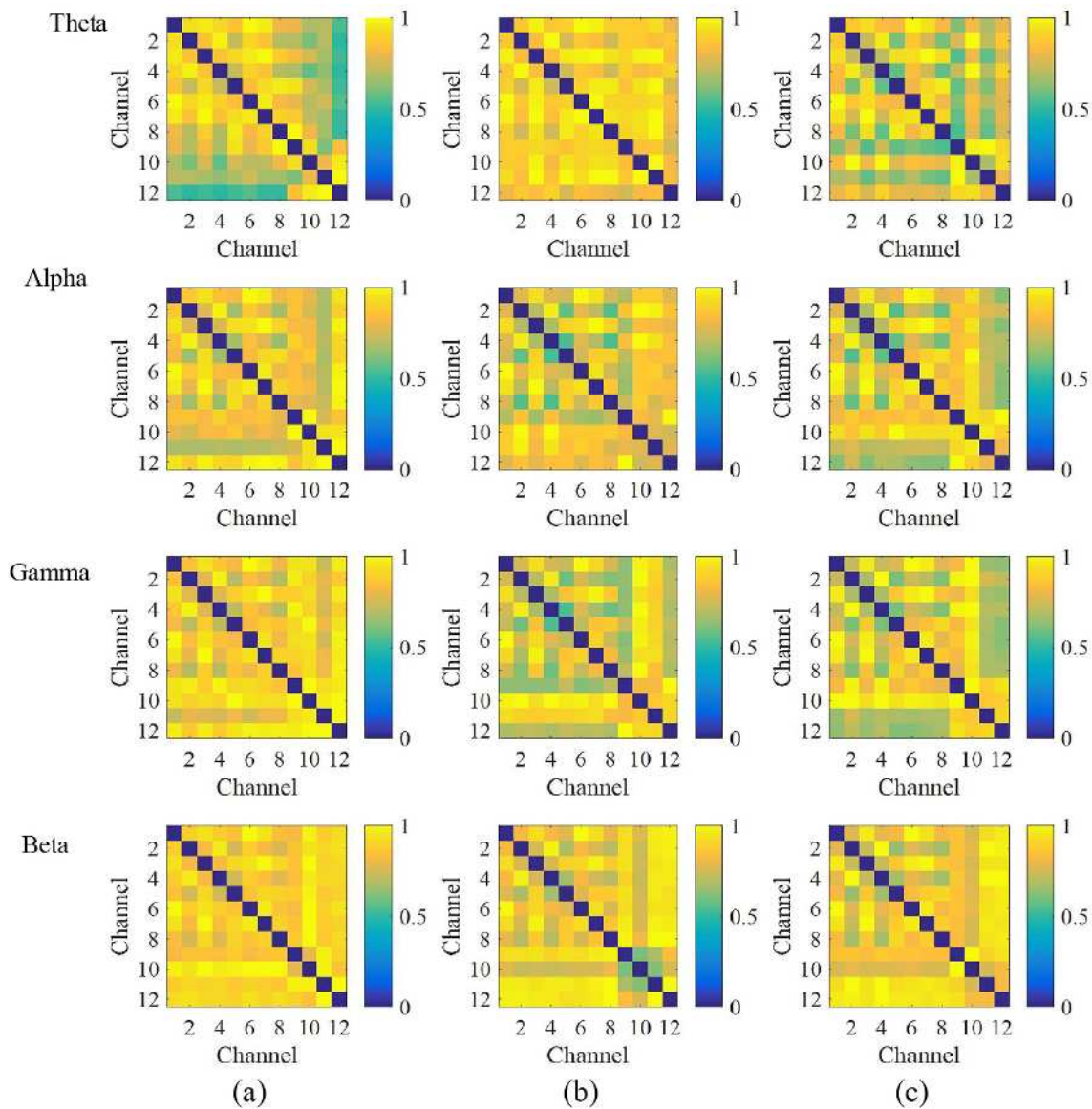
Fig. 3. Adjacency matrix's colormap of different motions using different frequency bands. (a) WF, (b) WE, and (c) CF.

to the statistical principles, the significance of differences can be judged by the value of F, so that when F>=F, there is a significant difference. We compared CW and LW of the network under three actions respectively, and the results show that the simplified models obtained by different motions demonstrated significant differences.

3.3. Model validation with small-world characteristics

Small-world networks have a high clustering coefficient and a small characteristic path length. We found that the cortical–muscular functional network in this study exhibited small-world characteristics by comparing it with ordered and random networks. The random network uses the ER random graph model. The ER model constructs the random graph algorithm as follows:

1. Initialization: given N nodes and connecting probability p[0,1].
2. Random edges: a. Select a pair of different nodes with no edges connected. b. Generate a random number r(0,1). c. If r Otherwise no edges are added. d. Repeat steps A-C until all node pairs have been selected once.

The small-world coefficient is a common index used to test the small-world network, and its calculation method is shown in formula 11–13.

$$\gamma = Cw_{exp}/Cw_{random} \tag{14}$$

$$\lambda = Lw_{exp}/Lw_{random} \tag{15}$$

$$\sigma = \gamma/\lambda \tag{17}$$

where Cw_{exp} and Lw_{exp} are the clustering coefficient and characteristic path length of the network to be analyzed, respectively, Cw_{random} and Lw_{random} are the clustering coefficient and characteristic path length of the random network, respectively. The network under study exhibits "small-world" characteristics for the small-world coefficient σ being greater than 1, and does not if otherwise.

In our experiment, we analyzed the small-world characteristics of the obtained functional networks. The weighted clustering coefficient Cw and weighted characteristic path length Lw of the cortical–muscular functional, ordered, and random networks were compared. The results are shown in Figs. 10 and 11, where "exp" represents the cortical–muscular functional network obtained by
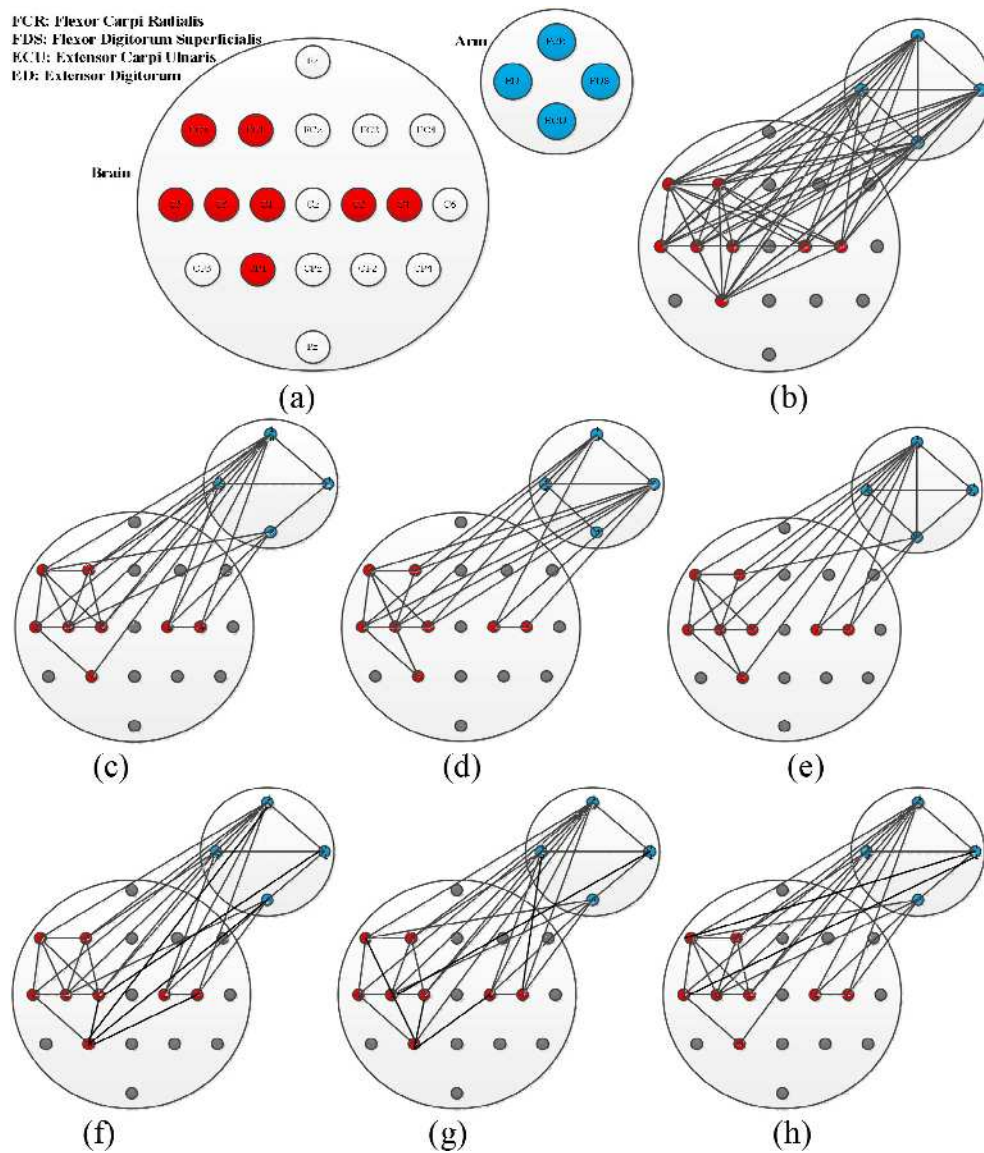
Fig. 4. Model diagram. (a) Introduction of the model diagram, (b) model diagram with a complete weighted edge, (c) model diagram of WF, (d) model diagram of WE, (e) model diagram of CF, (f) model diagram of WF, (g) model diagram of WE, and (h) model diagram of CF.
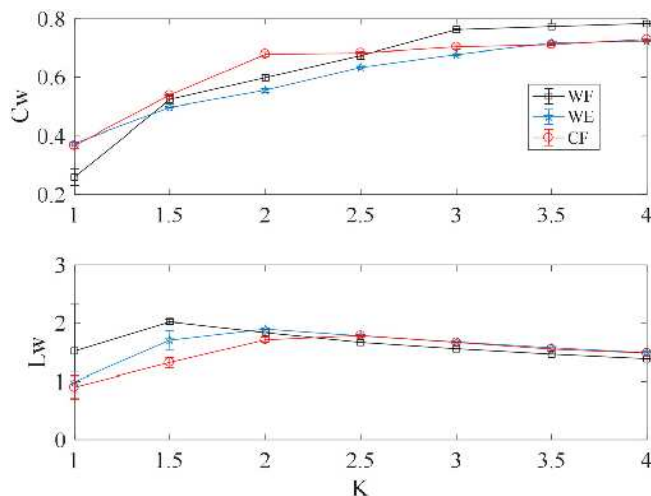

Fig. 5. Changes in Cw and Lw in different motions and different numbers of weighted edges.

the current experiment. The size and density of the three networks were the same. As shown in Figs. 10 and 11, we found that the weighted clustering coefficient Cw of the cortical–muscular functional network was much larger than that of the random network and not significantly different from that of the ordered network. The weighted characteristic path length Lw of the cortical–muscular functional network was larger than that of the random network and smaller than that of the ordered network. We have tested the small-world coefficient values of the network simplified by FWE and THR methods, as shown in Table 4. The results show that the constructed cortical–muscular functional network is an effective complex network with small-world characteristics. The characteristic path length between nodes is small, while the aggregation coefficient is still quite high, and its characteristics are between regular network and random network.

3.4. Model application in motion recognition

In the experimental process of the cortical–muscular functional network construction, we found that the networks obtained from WE, WF, and CF exhibited significant differences. As shown in
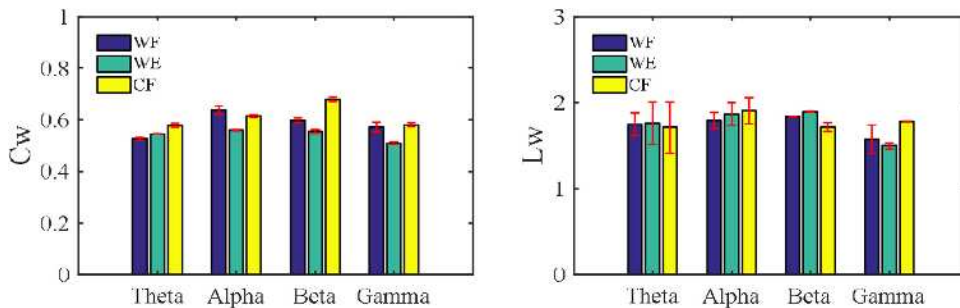
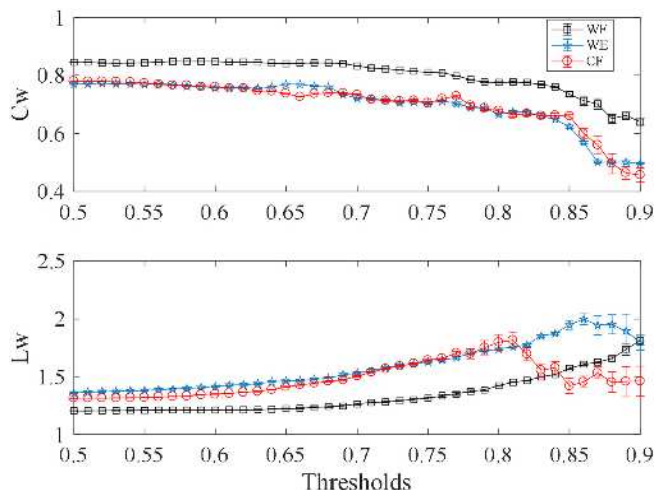**Fig. 6.** *Cw* and *Lw* in different frequency bands using FEW.

Fig. 7. Changes in *Cw* and *Lw* in different motions and thresholds.

Fig. 3 and Table 1, the adjacency matrices obtained from WE, WF, and CF were distinct. We increased the differences by simplifying the model. When we simplified the model by FEW and THR, we selected $K = 2$ as the number of the fixed weighted edge and $T = 0.85$ as the threshold on the basis of Figs. 5 and 7, respectively. Figs. 6 and 8 show the distinctions in different frequency bands. We then applied the network model to motion recognition now that the networks obtained from WE, WF, and CF have demonstrated significant differences.

We used the weighted clustering coefficient *Cw* and weighted characteristic path length *Lw* of the cortical–muscular functional network as features to recognize the three motions. The Fisher linear discriminant was selected as the classifier. Fig. 12(a)–(c) show the feature scatter diagram of every two motions. The feature of every two motions showed significant differences.

Table 5 shows the recognition rate of every two motions in the different model-simplified methods. The cortical–muscular functional network simplified by THR obtained high accuracy. The
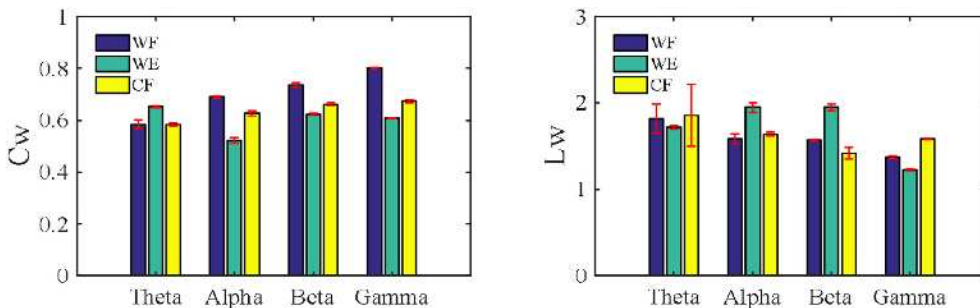
results demonstrate the effectiveness of the cortical–muscular functional network in practical applications.

In addition, we also used a three-layer Artificial neural network (ANN) to train a three-classification model. When setting the number of nodes in the ANN's hidden layer, we referred to the following three different empirical formulas.

$$m = \sqrt{n + l} + \alpha \tag{18}$$

$$m = \log_2 n \tag{19}$$

$$n = \sqrt{nl} \tag{20}$$

where *m* refers to the number of nodes in the hidden layer, *n* refers to the number of nodes in the input layer, *l* refers to the number of nodes in the output layer, and *α* refers to a constant between 1 and 10. We input the *Lw* and *Cw* of the network constructed under WE, WF and CF as features into our ANN. We used 90% of the collected data for training and 10% for verification. The accuracy of the final classification is shown in Table 6. It can be seen from Tables 5 and 6 that the network model simplified by THR has a higher classification accuracy.

In summary, the cortical–muscular functional network we constructed has small-world characteristics and can be used in practical applications after proper simplification. The study's results demonstrate the effectiveness of the networks and provide a foundation for subsequent research on the motion control mechanism of the central nervous system and the coordination mechanism of limb motion control.

4. Discussions and conclusions

Traditional brain functional networks focus on decoding cortical activity and trying to find functional connections between different cortical regions, while few studies use cortical and muscle functional networks to explore the body's motor mechanisms. Using previous research studies on brain functional networks and CMC, this paper adds EEG and EMG to the complex network for the first time, and proposes a cortical-muscular functional network to ver-

Fig. 8. *Cw* and *Lw* in different frequency bands using THR.

Table 2
CW differences between different actions.

	SS	df	MS	F	P-value	F crit
WE-WF	0.116389	1	0.116389	42.01822	1.29E-06	4.279344
WE-CF	0.173123	1	0.173123	86.6395	2.91E-09	4.279344
WF-CF	0.005613	1	0.005613	2.939031	0.099909	4.279344

Table 3
LW differences between different actions.

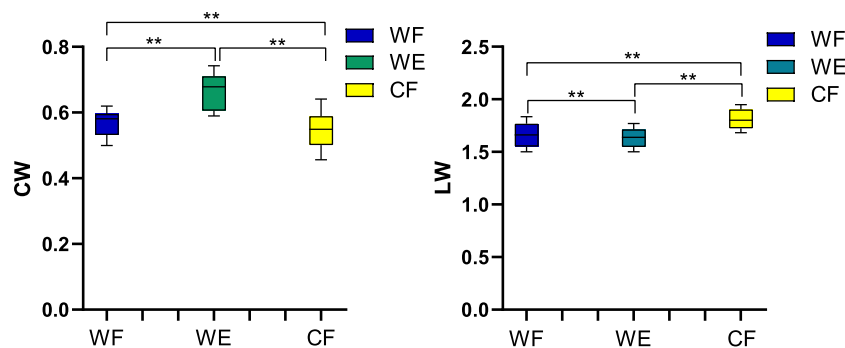|	SS	df	MS	F	P-value	F crit
WE-WF	0.006438	1	0.006438	0.538734	0.470374	4.279344
WE-CF	0.370689	1	0.370689	53.75321	1.85E-07	4.279344
WF-CF	0.279421	1	0.279421	23.73337	6.41E-05	4.279344

Fig. 9. The difference between CW and LW of the new adjacency matrix.

Table 4
Small world coefficients of the network under different actions.

	WF	WE	CF
σ (FWE)	1.9775	1.5445	2.8413
σ (THR)	1.8954	1.9652	2.6584

ify the information interaction between brain and muscle during human movement to explain the mechanism of movement. According to the function of brain region and the muscles of each arm, we selected 12 nodes of functional network and considered WC value as the indicator of the connection between nodes. When the subjects were performing three actions, the WC value of EEG-EMG was between EEG-EEG and EMG-EMG, and the WC value of WE, WF and CF also showed significant differences in different frequency bands. That is to say, different movements and frequency bands performed by human body can be distinguished by WC,

and the features of the functional network established thereby can reflect the movement intention of human body. When simplifying the constructed functional network, FWE method selects a fixed threshold value globally, while THR method sets a threshold value in accordance with the connection strength value at a certain position in the adjacency matrix and the position in the surrounding neighborhood. The method selected in this paper is the neighborhood block mean value method. Compared with FWE, THR is more flexible in the selection of thresholds with regional changes. Therefore, the network simplified by THR shows better characteristics, including small-world characteristics of the network and better separability, showing the potential of using cortical muscle activity to improve the traditional sEMG controller. The successful application of cortical muscle functional network in the decoding of human motor intention lays a foundation for the exploration of more effective methods of human behavior perception. In addition, our functional network can also study the pathology of
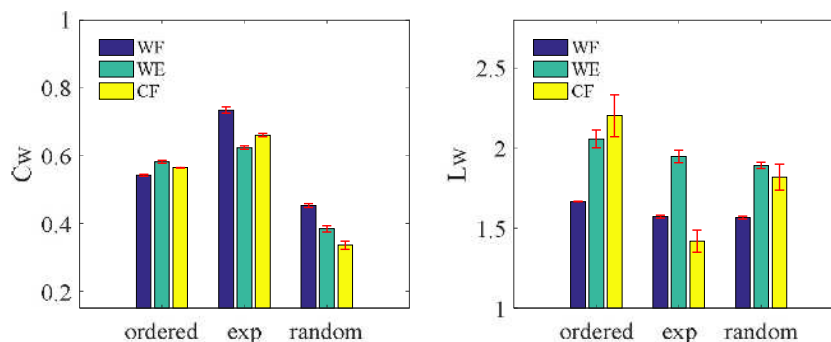

Fig. 10. Comparison of the cortical–muscular functional network simplified by THR, an ordered network, and a random network.
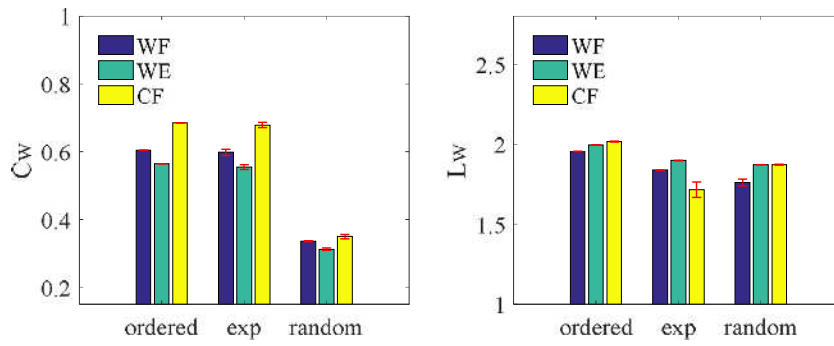
Fig. 11. Comparison of the cortical–muscular functional network simplified by FWE, an ordered network, and a random network.
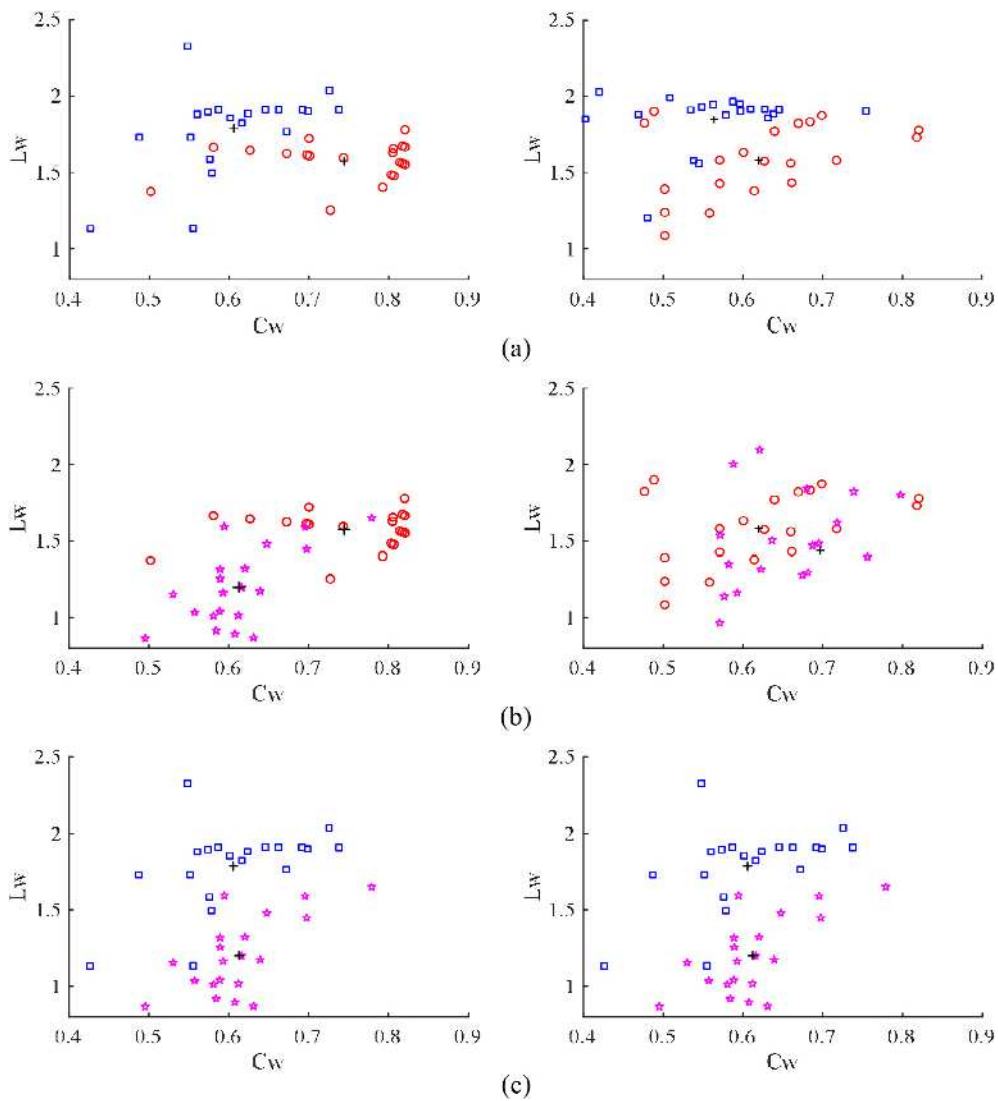

Fig. 12. Feature scatter diagram. The diagrams in the left and right represent the feature obtained from the cortical–muscular functional network simplified by THR and FEW, respectively. (a) WF-WE, (b) WF-CF, and (c) WE-CF.

Table 5
Recognition rate of every two motions in different model-simplified methods.

	WF versus WE	WF versus CF	WE versus CF
THR	90%	82.5%	95%
FEW	85%	60%	82.5%

Table 6
recognition rate of three motions in different model-simplified methods.

	WE	WF	CF
THR	94.2%	84%	88.3%
FWE	79.3%	70.2%	80.3%

X. Xi, Z. Sun, X. Hua et al. Neurocomputing 438 (2021) 248–258

patients with dyskinesia from the physiological mechanism, and develop scientific rehabilitation training methods to help patients recover as soon as possible.

One of the limitations of our approach is that the nodes may not be optimal for building a functional network. When selecting nodes, it is necessary to reasonably select acquisition channels in accordance with the functions of different brain regions and muscle regions. It is, however, a complex process. In future studies, in addition to the common THR and FWE, we also need to explore better optimization methods to simplify our functional networks.

CRediT authorship contribution statement

Xugang Xi: Conceptualization, Funding acquisition. **Ziyang Sun:** Writing - original draft, Writing - review & editing. **Xian Hua:** Visualization. **Changmin Yuan:** Software, Validation. **Yun-Bo Zhao:** Methodology. **Seyed M. Miran:** Supervision. **Zhizeng Luo:** Resources. **Zhong Lü:** Data curation.

Declaration of Competing Interest

The authors declare that they have no known competing financial interests or personal relationships that could have appeared to influence the work reported in this paper.
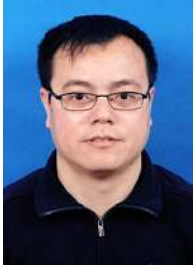
Acknowledgements

References

[1] F. Zhang, P. Li, Z.G. Hou, et al., sEMG-based continuous estimation of joint angles of human legs by using BP neural network, Neurocomputing 78 (1) (2012) 139–148.

[2] G.A. Lovell, P.D. Blanch, C.J. Barnes, EMG of the hip adductor muscles in six clinical examination tests, Phys. Ther. Sport. 13 (3) (2012) 134–140.

[3] S. Vanneste, J. J. Song, D. De Ridder, Thalamocortical dysrhythmia detected by machine learning, Nat. Commun. 9(1) (2018) Art. no. 1103.

[4] A. Mazaheri, K. Segaert, J. Olichney, et al., EEG oscillations during word processing predict MCI conversion to Alzheimer's disease, Neuroimage-Clin 17 (2018) 188–197.

[5] F. Lotte, L. Bougrain, A. Cichocki, et al., A review of classification algorithms for EEG-based brain–computer interfaces: a 10 year update, J. Neural Eng. 15(3) (2018), Art. no. 031005.

[6] P.L.C. Rodrigues, C. Jutten, M. Congedo, Riemannian procrustes analysis: transfer learning for brain-computer interfaces, IEEE T. Bio-Med. Eng. (2018) 1-1.

[7] J.J. Bird, A. Ekart, C.D. Buckingham, et al., Mental emotional sentiment classification with an eeg-based brain-machine interface, in: Proceedings of the International Conference on Digital Image and Signal Processing (DISP 19), 2019.

[8] L. Liu, X. Chen, Z. Lu, Development of an EMG-ACC-based upper limb rehabilitation training system, IEEE Trans. Neur. Syst. Reh. Eng. 25 (3) (Mar. 2017) 244–253.

[9] L.L. Chuang, Y.L. Chen, C.C. Chen, et al., Effect of EMG-triggered neuromuscular electrical stimulation with bilateral arm training on hemiplegic shoulder pain and arm function after stroke: a randomized controlled trial, J. Neuroeng. Rehabil. 14 (1) (2017) 122.

[10] K. Veer, Development of sensor system with measurement of surface electromyogram signal for clinical use, Optik 127 (1) (2016) 352–356.

[11] C. Castellini, A.E. Fiorilla, G. Sandini, Multi-subject/daily-life activity EMG-based control of mechanical hands, J. Neuroeng. Rehabil. 6 (1) (2009) 41.

[12] R.E. Johnson, K.P. Kording, L.J. Hargrove, et al., EMG versus torque control of human–machine systems: Equalizing control signal variability does not equalize error or uncertainty, IEEE Trans Neur. Syst. Reh. Eng. 25 (6) (2017) 660–667.

[13] D.J. Watts, S.H. Strogatz, Collective dynamics of 'small-world' networks, Nature 393(6684) (1998) 440–442.

[14] A.L. Barabási, R. Albert, Emergence of scaling in random networks, Science 286 (5439) (1999) 509–512.

[15] R. Ferri, F. Rundo, O. Bruni, et al., Small-world network organization of functional connectivity of EEG slow-wave activity during sleep, Clin. Neurophysiol. 118 (2) (2007) 449–456.

[16] G. Li, B. Li, Y. Jiang, et al., A new method for automatically modelling brain functional networks, Biomed. Signal Proces. 45 (2018) 70–79.

[17] F.A. Espinoza, V.M. Vergara, D. Reyes, et al., Aberrant functional network connectivity in psychopathy from a large (N= 985) forensic sample, Hum. Brain Mapp. 39 (6) (2018) 2624–2634.

[18] S. Boccaletti, V. Latora, Y. Moreno, et al., Complex networks: Structure and dynamics, Phys. Rep. 424 (4–5) (2006) 175–308.

[19] R. Bartsch, J. W. Kantelhardt, T. Penzel, et al., Experimental evidence for phase synchronization transitions in the human cardiorespiratory system, Phys. Rev. Lett. 98(5) (2007), Art. no. 054102.

[20] G. Pfurtscheller, F.H.L. Da Silva, Event-related EEG/MEG synchronization and desynchronization: basic principles, Clin. Neurophysiol. 110 (11) (1999) 1842–1857.

[21] S.N. Baker, E. Olivier, R.N. Lemon, Coherent oscillations in monkey motor cortex and hand muscle EMG show task-dependent modulation, J Physiol. 501 (1) (1997) 225–241.

[22] J.M. Kilner, S.N. Baker, S. Salenius, et al., Human cortical muscle coherence is directly related to specific motor parameters, J Neurosci. 20 (23) (2000) 8838–8845.

[23] J.M. Kilner, S. Salenius, S.N. Baker, et al., Task-dependent modulations of cortical oscillatory activity in human subjects during a bimanual precision grip task, Neuroimage 18 (1) (2003) 67–73.

[24] Y. Masakado, J. Ushiba, N. Tsutsumi, et al., EEG-EMG coherence changes in postural tasks, Electromyography Clin. Neurophysiol. 48 (1) (2008) 27–33.

[25] S. Salenius, K. Portin, M. Kajola, et al., Cortical control of human motoneuron firing during isometric contraction, J. Neurophysiol. 77 (6) (1997) 3401–3405.

[26] T. Mima, M. Hallett, Corticomuscular coherence: a review, J. Clin. Neurophysiol. 16(6) (1999), Art. no. 501-11.

[27] T. Mima, M. Hallett, Electroencephalographic analysis of cortico-muscular coherence: reference effect, volume conduction and generator mechanism, Clin. Neurophysiol. 110 (11) (1999) 1892–1899.

[28] S.-C. Bao, W.-W. Wong, T. Leung, R. K.-Y. Tong, Cortico-muscular coherence modulated by high-definition transcranial direct current stimulation in people with chronic stroke, IEEE Trans. Neural Syst. Rehabilitation Eng. PP (2018) 1-1.

[29] X. Chen, G. Xu, S. Zhang, L. min, The cortical-muscular functional coupling performance evaluation based on harmonic wavelet and symbolic phase transfer entropy, 2018, pp. 500–504.

[30] G. Pfurtscheller, C. Andrew, Event-related changes of band power and coherence: methodology and interpretation, J. Clin. Neurophysiol. 16(6) (1999), Art. no. 512.

[31] R.W. Thatcher, P.J. Krause, M. Hrybyk, Cortico-cortical associations and EEG coherence: a two-compartmental model, Electroencephalogr. Clin. Neurophysiol. 64 (2) (1986) 123–143.

[32] B.A. Conway, D.M. Halliday, S.F. Farmer, et al., Synchronization between motor cortex and spinal motoneuronal pool during the performance of a maintained motor task in man, J. Physiol. 489 (3) (1995) 917–924.

[33] C. Torrence, G.P. Compo, A practical guide to wavelet analysis, B Am. Meteorol. Soc. 79 (1) (1998) 61–78.

[34] J.P. Lachaux, A. Lutz, D. Rudrauf, et al., Estimating the time-course of coherence between single-trial brain signals: an introduction to wavelet coherence, Clin. Neurophysiol. 32 (3) (2002) 157–174.

[35] C. Andrew, G. Pfurtscheller, Event-related coherence as a tool for studying dynamic interaction of brain regions, Electroencephalogr. Clin. Neurophysiol. 98 (2) (1996) 144–148.

[36] E.P. Duff, T. Makin, M. Cottaar, et al., Disambiguating brain functional connectivity, NeuroImage 173 (2018) 5740–6550.

[37] M.E.J. Newman, The structure and function of complex networks, SIAM Rev. 45 (2) (2003) 167–256.

[38] E. Bullmore, O. Sporns, Complex brain networks: graph theoretical analysis of structural and functional systems, Nat. Rev. Neurosci. 10 (3) (2009) 186–198.

[39] A. Grinsted, J.C. Moore, S. Jevrejeva, Application of the cross wavelet transform and wavelet coherence to geophysical time series, Nonlinear Proc. Geoph. 11 (5/6) (2004) 561–566.

[40] C. Torrence, P.J. Webster, Interdecadal changes in the ENSO–monsoon system, J Climate. 12 (8) (1999) 2679–2690.

[41] A. Barrat, M. Barthelemy, R. Pastor-Satorras, et al., The architecture of complex weighted networks, P Natl. Acad. Sci. USA 101 (11) (2004) 3747–3752.

[42] M.E.J. Newman, Scientific collaboration networks. II. Shortest paths, weighted networks, and centrality, Phys. Rev. E. 64(2001), Art. no. 016132.

Xugang Xi is currently a professor with Hangzhou Dianzi University, Hangzhou, China. He received his B.S, M.S and Ph.D degrees from Hangzhou Dianzi University. His research interests include biomedical signal processing, human-robot interaction, and rehabilitation Robot.

Yun-Bo Zhao is currently a Professor with Zhejiang University of Technology, Hangzhou, China. He received his BSc degree in mathematics from Shandong University, Jinan, China in 2003, MSc degree in systems sciences from the Key Laboratory of Systems and Control, Chinese Academy of Sciences, Beijing, China in 2007, and PhD degree in control engineering from the University of South Wales (formerly University of Glamorgan), Pontypridd, UK in 2008, respectively. He has held postdoctoral positions with INRIA Grenoble, France, University of Glasgow, UK and Imperial College London, UK, respectively. His research interests include networked control systems, systems biology and artificial intelligence.

Ziyang Sun received his B.S degree from JiangSu KeJi University in 2018. He is working for a master's degree at Hangzhou Dianzi University. His research interests are biomedical signal processing and and Rehabilitation Robot.

Seyed M. Miran received a PhD degree in systems engineering and a master of science in statistics from University of Akron in Ohio, USA. He is currently a postdoctoral fellow with Biomedical Informatics Center, George Washington University, Washington, DC, USA. His current interests are system design, applied probability and statistics, multimodal human–computer interaction.

Xian Hua received his M.S degree from Zhejiang Chinese Medical University in 2012. Xian Hua is currently a clinician with Jinhua People's Hospital. Her current research interests include electroencephalograph and application of artificial intelligence in medical field.

Zhizeng Luo received the Ph.D. degree in Zhejiang University in 1998. He is a Professor in Hangzhou Dianzi University. His current research interests include pattern recognition, biomedical engineering and rehabilitation Robot.

Changmin Yuan received his B.S degree from Jiangnan University in 2017. He is working for a master's degree at Hangzhou Dianzi University. His research interests are biomedical signal processing and and Rehabilitation Robot.

Zhong Lü received his bachelor's degree in Wenzhou Medical University in 1988. He is a Professor in Affiliated Dongyang Hospital of Wenzhou Medical University. His current research interests include application of artificial intelligence in medical field, hospital management.